Journal of Advanced Research 65 (2024) 73–87

Contents lists available at ScienceDirect

Journal of Advanced Research

journal homepage: www.elsevier.com/locate/jare

Targeting acid ceramidase enhances antitumor immune response in colorectal cancer

Yadu Vijayan [a,b], Shirley James [a], Arun Viswanathan [a,b], Jayasekharan S Aparna [a], Anu Bindu [a], Narayanan N Namitha [a], Devasena Anantharaman [a], Manendra Babu Lankadasari [a,1], Kuzhuvelil B Harikumar [a,*]

[a] Cancer Research Program, Rajiv Gandhi Centre for Biotechnology (RGCB), Thiruvananthapuram, 695014, India
[b] Manipal Academy of Higher Education (MAHE), Manipal, 576104, India

HIGHLIGHTS

- Acid ceramidase (ASAH1) is an enzyme in sphingolipid metabolism that converts pro-survival ceramide into sphingosine and its role in colorectal cancer (CRC) is not known.
- ASAH1 is over expressed in human murine CRC and silencing ASAH1 induces immunological cell death (ICD) in CRC cell lines.
- ASAH1 silencing also modulate the glutathione system and induces mitochondrial stress.
- Combination of ASAH1 inhibitor along with check point therapy (anti PD-1) sensitize the tumor cells to immunotherapy.

GRAPHICAL ABSTRACT

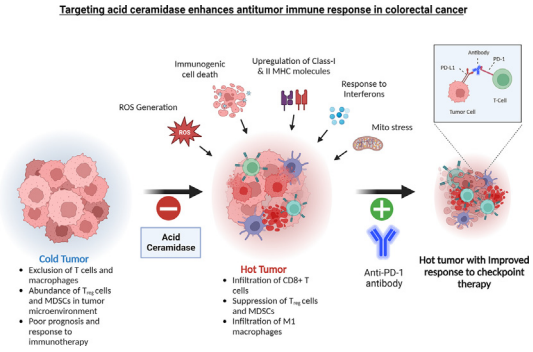

ARTICLE INFO

Article history:
Received 27 October 2023
Revised 14 December 2023
Accepted 16 December 2023
Available online 21 December 2023

Keywords:
Colorectal cancer
Acid ceramidase
LCL-521
Checkpoint inhibitor
Immunological cell death
T cells

ABSTRACT

Introduction: Acid ceramidase (hereafter referred as ASAH1) is an enzyme in sphingolipid metabolism that converts pro-survival ceramide into sphingosine. ASAH1 has been shown to be overexpressed in certain cancers. However, the role of ASAH1 in colorectal cancer still remain elusive.
Objective: The present study is aimed to understand how ASAH1 regulates colorectal cancer (CRC) progression and resistance to checkpoint inhibitor therapy.
Methods: Both pharmacological and genetic silencing of ASAH1 was used in the study. In vitro experiments were done on human and mouse CRC cell lines. The *in vivo* studies were conducted in NOD-SCID and BALB/c mice models. The combination of ASAH1 inhibitor and checkpoint inhibitor was tested using a syngeneic tumor model of CRC. Transcriptomic and metabolomic analyses were done to understand the effect of ASAH1 silencing.
Results: ASAH1 is overexpressed in human CRC cases, and silencing the expression resulted in the induction of immunological cell death (ICD) and mitochondrial stress. The ASAH1 inhibitor (LCL-521),

Abbreviations: AML, Acute Myeloid leukemia; APC, Antigen Presenting Cells; CDK, Cyclin-Dependent Kinases; CTLA4, Cytotoxic T-lymphocyte–associated Antigen 4; DAMP, Damage-Associated Molecular Patterns; DSS, Dextran Sodium Sulfate; ER, Endoplasmic Reticulum; FFPE, Formalin Fixed Paraffin Embedded; GBM, Glioblastoma Multiforme; GEPIA, Gene Expression Profiling Interactive Analysis; HMGB1, High Mobility Group Box 1; IFN, Interferons; MHC, Major Histocompatibility Complex; MtDNA, Mitochondrial DNA; OCR, Oxygen Consumption Rate; PCNA, Proliferative Cell Nuclear Antigen; PD-1, Programmed Cell Death 1; TCGA, The Cancer Genome Atlas Program; Treg, Regulatory T cells.

* Corresponding author.
E-mail address: harikumar@rgcb.res.in (K.B Harikumar).
[1] Current address: Memorial Sloan Kettering Cancer Center, New York, NY 10065, USA.

https://doi.org/10.1016/j.jare.2023.12.013

either as monotherapy or in combination with an anti-PD-1 antibody, resulted in reduction of tumors and, through induction of type I and II interferon response, activation of M1 macrophages and T cells, leading to enhanced infiltration of cytotoxic T cells. Our findings supported that the combination of LCL-521 and ICIs, which enhances the antitumor responses, and ASAH1 can be a druggable target in CRC.

Introduction

Targeting the tumor microenvironment (TME) and augmenting the host immune response are emerging strategies for managing cancer [1,2]. Tumors have an inherent capacity to create an overall immunosuppressive environment and thereby escape from immunosurveillance that causes significant obstacles to effective antitumor immunity and immunotherapy based treatment strategies [3]. Therefore, improving the effector function of tumor-specific T cells is a key determinant for successful immunotherapy against various types of cancers [4,5]. Immune checkpoint inhibitor (ICI) therapy is one form of immunotherapy approach with limited success rates in some cancers, including colorectal cancer [6–8]. Treatment with anti-PD1/PD-L1 antibodies is one such approach that can modulate T cell functions in the TME [9] and factors such as mutational burden, presentation of neoantigens, IFN-γ gene signature, the ratio of CD8/Treg cells, etc., regulate the efficacy of the treatment [10]. Tumors lacking such factors often fail to respond to ICI therapy [11]. Currently, agents (examples: radiation therapy, anthracyclines, and oxaliplatin) which can induce immunogenic cell death (ICD) is gaining interest because these molecules can improve the recruitment of T cells and activate antigen presentation by dendritic cells [12,13].

Acid ceramidase (N-acylsphingosine deacylase, EC 3.5.1.23) a key enzyme in the sphingolipid metabolism, converts pro-survival ceramide into sphingosine, which in turn is converted into Sphingosine-1-Phosphate (S1P) [14,15]. A deficiency of ASAH1 activity resulted in Farber disease [16] and spinal muscular atrophy with progressive myoclonic epilepsy (SMA-PME) [17]. There is an S1P-ceramide rheostat which is one of the mechanisms that determines the fate of the cell, where S1P favors cell survival [18]. ASAH1 is overexpressed in a subset of cancers such as head & neck [19], prostate [20], pancreatic [21], AML [22], and GBM [23]. There is an inverse correlation between ASAH1 expression and tumor suppressor PTEN expression [24]. In colorectal cancer (CRC), there is a correlation between heightened expression of ASAH1 in epithelium and stroma in tumor samples and local recurrence rate [25]. In rectal cancer, ASAH1 modulates the sensitivity to radiation therapy, and inhibiting ASAH1 expression enhances radio sensitivity and apoptosis [26].

Here, we report that ASAH1 is highly overexpressed in CRC, and targeting ASAH1 leads to the induction of immunological cell death, enhanced antigen presentation, and mitochondrial stress. Further ASAH1 inhibitor sensitizes colorectal cancer to an immune checkpoint inhibitor, resulting in a better treatment response.

Methods

The sources of different reagents and kits were described in **supplementary methods**.

Cell culture, chemicals and tissue microarrays

HCT116, SW480, SW620, and CT-26 cells were initially procured from American Type Culture Collection. HCT116, SW480, and SW620 were maintained in DMEM and CT26 in RPMI, with 10 % fetal bovine serum and antibiotics. Cells were checked for mycoplasma contamination at regular intervals using a kit from Agilent. The CRC tissue microarrays were procured from US Biomax. LCL-521 was synthesized at The Lipidomics Shared Resource of the Medical University of South Carolina (MUSC).

Animals

NOD.CB17-Prkdc^{scid}/J mice (6–8-week-old, hereafter referred to as NOD-SCID) and BALB/c (6–8 week old) mice were obtained from Jackson laboratories (USA) and kept in individually ventilated cages (IVCs) with standard rodent chow, water *ad libitum*, and a 12 h light/dark cycle. All the experiments were performed during the light cycle. The animal experiment protocol got prior approval from the Institutional Animal Ethics Committee (IAEC) of RGCB and followed the rules and regulations prescribed by the Committee for Control and Supervision of Experiments on Animals (CCSEA), Government of India.

Immunohistochemistry (IHC)

IHC was done as described earlier with minor modifications [27]. Tissue sections were first deparaffinized and hydrated using descending grades of alcohol. For antigen retrieval, tissue sections were dipped in citrate buffer (pH 6.0), followed by exposure to steam heat. After cooling and subsequent washes, peroxidase activity was inhibited using a peroxidase quencher from Pathnsitu HRP/DAB detection system kit and blocked using an animal free blocker. The primary antibodies for ASAH1 at 1:400 dilution, PCNA, c-Myc, and cyclin D1 at 1:100 dilution each were added and incubated overnight at 4 °C. The following day, tissue sections were covered with poly excel target binder followed by poly excel HRP using a kit from Pathnsitu HRP/DAB detection system kit. Counterstaining was done with hematoxylin, and the tissue sections were mounted with DPX. Images were captured using the Nikon Eclipse Ni-E microscope at 20X magnification.

Cell proliferation assay

This was done using an MTT assay, as described earlier [28]. Briefly, 5×10^4 cells were plated in 96-well plates, and treated with different concentrations of drug for indicated time points. 20 µL of MTT (5 mg/mL) was added to each well and incubated for 4 h. After removing the media, the formazan crystals were dissolved in DMSO, and optical density was measured at 595 nm using a spectrophotometer.

Annexin V FITC staining

The staining was done using a commercially available kit as per the instruction of the manufacturer (Abgenex). Briefly, after the LCL-521 treatment, cells were trypsinized and resuspended in 1X binding buffer, and 5 µL Annexin-FITC was added and incubated in the dark for 15 min at room temperature. This was followed by the addition of 5 µL of Propidium Iodide (1 mg/mL) and incubated in the dark for 5 min. The cells were filtered using

40 μm cell strainer and analyzed in BD FACS ARIA-III flow cytometer.

RNA extraction and quantitative RT-PCR (q-PCR)

The methodology as previously described was followed [29]. The primer sequences used were PSMB8 (F: ATGGCGTTACTGGATCTGTGC, R: CGCGGAGAAACTGTAGTGTCC), B2M (F: TTCTGGTGCTTGTCTCACTGA, R: CAGTATGTTCGGCTTCCCATTC), Anx A1 (F: AAGCAGGCCCGTTTTCTTGAA, R: GCAACATCCGAGGATACATTGA), LGMN (F: TGGACGATCCCGAGGATGG, R: CGGTGGATGATCTGGTAGGC). ASAH1 Sigma-Aldrich #NM_019734.

Plasmids and shRNAs

We used predesigned and validated shRNA glycerol stocks from Sigma Aldrich to generate ASAH1 knockdown cells. The following ASAH1 shRNA clones were used for mouse cell lines (TRCN0000101471, TRCN0000101472, and TRCN0000101473) and for human cell lines (TRCN0000029399 and TRCN0000029402). The glycerol stocks were grown in ampicillin containing LB broth, and plasmids were isolated using NucleoBond Xtra Midi kit (MN). Transfection was carried out using a 3rd generation lentiviral transfection system. Selection of ASAH1 knockdown cells (ASAH1-KD) was done using 2 μg/ml puromycin, and knockdown efficiency was verified using kick-start primers through qPCR analysis. TRCN0000101471 and TRCN0000029399 were selected for subsequent studies.

Determination of reduced glutathione (GSH)

Cells were lysed by repeated cycles of freeze-thawing and mixed with 125 μL of 25 % TCA (Trichloroacetic acid) and cooled on ice for 5 min, followed by further dilution by adding 600 μL of 5 % TCA and then subjected to centrifugation at 3000g for 5 min to pellet down the precipitate. 150 μL of supernatant was mixed with 350 μL of sodium phosphate buffer (0.2 M, pH 8.0) and 1.0 mL of DTNB (Ellman's Reagent) (5,5-dithio-bis-(2-nitrobenzoic acid) (0.6 mM in 0.2 M, pH 8.0 phosphate buffer). The yellow color obtained was measured at 412 nm against a blank that contained 5 % TCA in place of supernatant. The GSH concentration was calculated and expressed as nmol/mg of protein [30].

Determination of glutathione peroxidase (GPx) activity

Glutathione peroxidase depletes H_2O_2 in the presence of glutathione (GSH). The remaining.

GSH is measured using 5,5-dithio-bis-(2-nitrobenzoic acid) (DTNB), which gives a colored complex. The reaction mixture contained 50 μL (5 mM) GSH, 800 μL of 0.1 M phosphate buffer (pH 7.0) with 1 mM EDTA, 50 μL sodium azide (25 mM), 50 μL (10 %) tissue/cell extract, and 50 μL of H_2O_2 (2.5 mM) in a total volume of 1 mL for determining the enzyme activity after 10 min. The reaction mixture was incubated at 37 °C for 10 min. The reaction was stopped by the addition of 1.0 mL of 1.67 % of meta- phosphoric acid and centrifuged for 15 min at 3000 rpm. To determine the enzyme activity at zero minutes, 1 mL of 1.67 % *meta*-phosphoric acid was added immediately to the reaction mixture before incubation. To about 1 mL of supernatant, 1 mL of 0.4 M Na_2HPO_4 and 0.5 mL DTNB (1 mM) were added. Incubation was carried out at 37 °C for 10 min, and absorbance was measured at 412 nm [31].

Metabolomic analysis

The samples ($10x10^6$ cells) were lysed by freeze-thawing followed by sonication. Proteins in the samples were precipitated by resuspending the samples in 700 μL methanol. Subsequently, 600 μL of chloroform was added to each sample, followed by vortexing and centrifugation at 14,000 g for 15 min at 4 °C.The aqueous phase was transferred into a fresh tube and 600 μL of acetonitrile was added, vortexed and incubated at −80 °C for 2 h. The samples were centrifuged at 14, 000 g at 4° C for 20 min. The resulting supernatant was then dried at room temperature with the SpeedVac concentrator and reconstituted in a 100 μL solvent containing 50 % methanol and 0.1 % formic acid. All the samples were analyzed in both reverse phase positive and reverse phase negative acquisition modes. Liquid chromatography system (ACQUITY UPLC) coupled to a Synapt G2 High-Definition MS™ System (Waters) (HDMSE System) was used for untargeted metabolomics analysis. The analytical column used was ACQUITY UPLC HSS T3 1.8 μm 2.1 x 100 mm. For the Reversed-Phase Liquid Chromatography (RPLC) the mobile phase consisted of two solvent components; aqueous solvent (A) containing 0.1 % formic acid in water and organic solvent (B) containing 0.1 % formic acid in acetonitrile for both positive and negative acquisition. The chromatography gradient was 0 min, 1 % B; 1 min, 1 % B; 16 min, 100 % B; 20 min, 100 % B, and 22 min, 1 % B. Data were acquired in both positive and negative modes in resolution mode (MSE) with electrospray ionization. MassLynx4.1 SCN781 (Waters) was used for data acquisition and Progenesis QI (Non-linear dynamics, Waters) was employed for data analysis. The ion abundance was used for the relative quantification of metabolites. An online mass correction was done using leucine encephalin for ESI positive and ([M + H] + =556.2766) and ESI negative ([M−H]- 554.2620) mode. The databases used were KEGG- HMDB and MMDB. [32].

Realtime analysis of cellular energy metabolism

Seahorse XF Extracellular Flux Analyzer (Agilent Technologies) was used to perform mito stress assay in a 96-well format. 2500 cells were plated per well in complete media and cells were treated with different concentrations of LCL-521 after 24 h. The cells were washed and incubated with assay medium (XF-DMEM containing 10 mM glucose, 1 mM pyruvate, and 2 mM L-Glutamate) for 1 h at 37 °C and then incubated in a CO_2-free incubator to guarantee precise measurements of extracellular pH. OCAR and ECAR measurements were taken following the manufacturer's protocol. The data were collected in basal condition and in response to 1.5 μM oligomycin (OLI), 0.5 μM Fluorocarbonyl-cyanide-phenylhydra zone (FCCP), and 0.5 μM rotenone/antimycin A (Rtn/AA) [33].

HMGB1 release assay

HMGB1 detection was done using the detection kit from Elabscience. $2X10^5$ cells were plated in 6 well plates, and after LCL-521 treatment for 24hr culture, the supernatant was used for the assay.

ATP release detection

The luminescent Cell Viability Assay kit from Pierce was used for ATP detection as per the instructions of the manufacturer (Promega). The culture supernatant was used to detect released ATP and luminescence was measured using Varioskan LUX multimode microplate reader.

Reactive oxygen species (ROS) analysis

2X10^5 cells in 6 well plates were treated with LCL-521 for 24 h. After the treatment, cells were stained with 5 μM H2DCFDA, incubated in the dark for 30 min, cells are trypsinized and filtered through a cell strainer, and analyzed in BD FACS ARIA-III flow cytometer. For assays in the presence of N-Acetyl-L-cysteine (NAC), the cells were pre-treated with 5 mM NAC for 2 h, followed by drug treatment.

LDH assay

LDH Assay was done on cell culture supernatant to detect the presence of LDH in the media of ASAH1 knockdown, and LCL-521 treated HCT116 and CT26 cells using EZcount™ LDH Cell Assay Kit, following manufactures protocol (Himedia).

Cell cycle analysis

The analysis was done as described previously [27]. Briefly, cells were plated at a density of 3×10^5 in a 6-well plate and after 24 h cells were treated with LCL-521 for 24 h. The cells were stained with propidium iodide (100 μg/mL) (Sigma) and analysis was carried out by BD FACS ARIA-III system.

Cell migration assay

The analysis was done as reported previously [27]. Briefly, cells (1×10^5) were plated in 12-well plates and allowed to reach 90 % confluence. A wound was made using a 200 μL tip and the floating cells were carefully removed through PBS washing. Further, cells were treated with LCL-521 and the cells were monitored for the rate of wound closure. 100X images were taken at 0, 24 and 48 h using a phase contrast microscope.

Preparation of single cell suspension

The dissected tumor tissues were minced and treated with type IV collagenase (2 mg/mL) for 2 hrs. After centrifugation, the pellet was treated with trypsin, and after washing, the pellet was incubated with RBC lysis buffer. After centrifugation, the suspension was then passed through a 40 μm cell strainer to remove the debris to make it a single cell suspension. The cells were then counted using a hemocytometer, and cells were blocked with Fc block followed by staining with different antibody cocktails (details are given in **supplementary methods**) on ice for 1 h with intermittent mixing to prevent cells from settling. The cells were analyzed in BD FACS ARIA-III flowcytometer, and data analysis was done using FlowJo™ v10.

Xenograft models in mice

HCT116 or CT26 cells (7x10^5 cells, 100 μL in serum free media) were injected into the right flank of either NOD-SCID or BALB/c mice. The animals were grouped into the following. Group I: Vehicle (Double distilled water, 100 μL, *i.p*, daily), Group II: LCL-521 (50 mg/Kg body wt, *i.p*, daily), and Group III: ASAH1-KD cells. For the combination study, BALB/c mice were injected with CT26 cells (7 x10^5 cells, 100 μL volume in serum free media) to the right flank and divided into the following groups: Group I: Vehicle (Double distilled water, 100 μL, *i.p*, daily), Group II: LCL-521 (50 mg/Kg body wt, *i.p*, daily) and Group III: anti-PD1 mouse antibody (200 μg/dose/week, *i.p*) and Group IV: LCL-521 (50 mg/Kg body wt, *i.p*, daily) and anti-PD1 mouse antibody (200 μg/dose/week, *i.p*). Animals were sacrificed 18–20 days after tumor implantation, tumors from the flank were excised, and the final tumor volume was measured as V = (length × width2) / 2, where V is the tumor volume. A part of the tumor was used for single cell preparation; another part was fixed in formalin and used for immunohistochemical analysis; the remaining portion was snap frozen in liquid nitrogen for protein and RNA extraction.

Transcriptomic analysis

RNA was extracted using RNeasy Mini Kit (details) following the manufacturer's protocol. The RNA quality assessment was done using the RNA ScreenTape System in a 4150 Tape Station System. 1 μL RNA sample was mixed with 3 μL of RNA ScreenTape Sample buffer, then heat denatured at 72 °C for 3 min, followed by immediate placement on ice for 2 min. The sample was then loaded onto the Agilent 4150 TapeStation instrument to determine the integrity of RNA using the RNA integrity number (RIN) assigned by the software. The sequence data were generated using Illumina NovaSeq 6000 using fastp v0.20; sequence reads were processed to remove adapter sequences and low quality bases. The QC passed reads were mapped onto the Mus musculus genome using STAR v2 aligner. Using feature-counts software, gene level expression values were obtained as read counts. Spearman Rank Correlation and Principal Components Analysis were used to check whether the biological replicates are corroborating with each other with respect to their expression profiles. Spearman Rank correlation is used for Gaussian distribution, such as gene expression data which shows negative binomial distribution. The biological replicates were grouped as Reference and Test for differential expression analysis. Differential expression analysis was carried out using DESeq2 package after normalizing the data using the relative log expression normalization method. Genes with absolute log2 fold change ≥ 1 and adjusted p-value ≤ 0.05 were considered significant. The UpSetR R package was used to generate plots showing overlapping significant genes between conditions. The heat maps were generated by using normalized expression values for each sample for a given gene. Gene ontology and Pathway Analysis Over representation analysis for biological process, Molecular function, Cellular components, and KEGG Pathway was performed using Cluster Profiler R Bioconductor package. Gene Ontology (GO) and pathway terms with multiple test adjusted p-value ≤ 0.05 are considered significant.

The upregulated gene signatures were calculated using online software pantherDB.

Statistical analysis

The data were expressed as either mean ± SD or mean ± SEM and statistical analyses were done using GraphPad Prism 10 (GraphPad software, CA, USA) between two groups were performed either with unpaired two-tailed Student's *t*-test or ANOVA. p value < 0.05 was considered statistically significant. Chi-squared tests to examine the association between ASAH1 expression and clinical parameters and statistical analysis was performed using STATA software, version 15 (Stata Corp, College Station, TX). All reported p-values are two-sided and the significance level was set at < 0.05.

Results

ASAH1 is upregulated in human CRC, murine colitis and CRC

To elucidate the role of ASAH1 in CRC, we first analyzed the expression of ASAH1 using an immunohistochemical approach in a human CRC tissue array. We used 212 adenocarcinomas and matching adjacent normal samples. The descriptive characteristics

of the study samples are shown in **Supp Table 1**. The staining was done using an antibody specific to ASAH1, and scoring (scale of 1–4) was performed in a blinded manner. We tested whether the expression was associated with a cancer diagnosis in a logistic regression model; control (adjacent normal) was considered the outcome variable, and IHC expression levels 1 to 4 were the predictor variable. Odds ratios and 95 % confidence intervals were computed with and without adjustment for other variables, including testing batch and sex. We noted that high levels of expression are associated with an increased risk of being a case. Conversely, colon tissues with high ASAH1 expression are 400 times more likely to be diagnosed as cancerous than the adjacent normal (Fig. 1 A and B and **Supp Table 2**). Next, the TCGA data set and GTEx for normal samples were analyzed to check the expression of ASAH1 in CRC. GEPIA box plots of key gene expression levels showed that ASAH1 is significantly upregulated in CRC cases (n = 275) as compared to normal (n = 349) samples (Fig. 1C). Having confirmed that ASAH1 is upregulated in human CRC cases, we further investigated the status of ASAH1 in murine cancer models. From our tissue archives [28,34], we selected both frozen and FFPE tissue samples of mouse DSS-induced colitis, Azoxymethane (AOM) driven CRC and AOM induced DSS promoted colitis-associated cancer (CAC) samples, and ASAH1 expression was analyzed using qRT-PCR and IHC. As shown in Fig. 1D (left panel), ASAH1 mRNA levels were significantly increased in colitis, CRC, and CAC samples. Similarly, IHC staining also demonstrated that, compared to the normal colon, the ASAH1 expression is elevated in AOM and AOM-DSS samples (Fig. 1D right panel). Taken together, our data concludes that ASAH1 is overexpressed and associated with the pathogenesis of CRC.

Knockdown of ASAH1 expression inhibited tumor growth in immunocompetent mice

We sought to understand whether downregulating ASAH1 expression affected the tumor progression and decided on the strategy to silence ASAH1 expression through a genetic and pharmacological approach. ASAH1 stable knockdown cell lines (HCT116 and CT26) were generated using a lentiviral approach using different shRNA clones (**Supp Fig. 1** A–B). To attain pharmacological silencing of ASAH1, we used LCL-521, a specific inhibitor of ASAH1 [35]. Initially, HCT116 and CT26 WT (vector) and ASAH1-KD cells were injected into NOD-SCID mice, and one group of mice injected with WT cells was treated with LCL-521. Interestingly we did not observe any significant regression in the tumor after ASAH1 silencing in immunodeficient mice strains (Fig. 2 A–B). This prompted us to test the effect in immunocompetent (syngeneic) mice model. Both ways of silencing ASAH1 significantly reduced the final tumor volume and tumor weight indicating the role of the host immune system in the process (Fig. 2C). Immunohistochemical analysis of proliferative markers (PCNA and Cyclin D1) and H&E staining was done in tumor samples. There was more positive PCNA and Cyclin D1 staining in vehicle-treated groups compared to ASAH1-KD groups (Fig. 2D). This indicates that ASAH1 regulates cell proliferation by modulating PCNA and Cyclin D1 expression. We also analyzed the surface level expression of CD45, CD11b, and CD8 in single-cell suspensions from tumor samples using FACS. CD11b is a key regulator of pro-inflammatory immune responses within the tumor microenvironment and prevents tumor progression [36]. Higher infiltration of CD8+T cells is associated with improved survival in CRC patients [37]. We noticed that expression of CD11b and CD8 were elevated after LCL-521 treatment and in ASAH1-KD group, further confirming that ASAH1 mediates the effect through modulation of the host adaptive immune system (Fig. 2E).

ASAH1 downregulation resulted in immunological cell death and release of DAMPs in CRC cell lines

The *in vivo* studies indicating the involvement of adaptive immune response prompted us to hypothesize that LCL-521 could potentially induce immunological cell death (ICD). We first checked the cytotoxicity of LCL-521 in different human and murine CRC cell lines for 24hrs, and IC_{50} varies between the 20–40 μM range (Fig. 3A). LCL-521 was found to be cytotoxic in all the tested cell lines. Extracellular Lactate dehydrogenase (LDH) released due to damage to the plasma membrane serve as a marker for apoptosis [38]. We measured the LDH levels and observed that LCL-521 treatment released more LDH as compared to vehicle treated cells in HCT116, CT26 and SW 620 cell lines (Fig. 3B and **Supp Fig. 2**A). The treatment with LCL also resulted in cell cycle arrest in SubG1 phase (Supp 2B-C). To further confirm it as apoptosis, we used Annexin V-propidium iodide based staining of the cells. Flow cytometry based quantification of the cell population indicated that LCL-521 induced apoptosis in dose dependent manner (Fig. 3C). To study the role of ASAH1 in cell migration, we performed a wound healing assay for two time points (24 and 48hrs). We noticed a marked inhibition of migration potential in cells treated with LCL521 as evident from the decrease in wound closure area (Supp 3A-B). Based on these studies, we determined the doses below the IC_{50} values for studying the ICD. We checked the surface level expression of MHC II (HLA DR) involved with APCs, and increased expression of MHC class II might increase the recognition of a tumor by the host immune system. LCL-521 treatment resulted in an increased surface expression of MHC II in HCT116 (**Supp Fig. 4**A) and CT26 (Fig. 3D- right panel) when analyzed through flow cytometry. Similarly, we also observed that MHC I (H2-Kb) expression was elevated in CT26 after ASAH1 silencing (Fig. 3D-left panel). Next, we analyzed the classical markers of ICD and the release of DAMPs [39,40]. Calreticulin (CRT) is an ER-associated chaperone involved in MHC-I dependent antigen processing. During ICD, CRT is expressed on the cell surface and acts as a signal to APCs [41]. The LCL-521 treatment resulted in an increased cell surface expression of calreticulin (Fig. 3E and **Supp Fig. 4**B). While the cell is undergoing ICD; HMGB1, nuclear non-histone chromatin-binding protein is released from the nucleus into the surroundings of dying cells [42]. Using the ELISA, we quantified the secretion of HMBG1 in CT26 cells and noticed an increased secretion after LCL-521 exposure for 24 h (Fig. 3F). Concomitantly the induction of ICD is also associated with the secretion of ATP from dying cancer cells to the extracellular milieu [43]; we also observed the same in our ASAH1 silenced cells (Fig. 3G and **Supp Fig. 4**C). These results, for the first time, confirmed that ASAH1 downregulation resulted in the induction of ICD in CRC cell lines, leading to more activation of immune cells and enhanced antigen presentation by APCs, thereby promoting the antitumor immune response.

ASAH1 silencing alters the metabolome profiles in CRC cell lines

ASAH1 is a key enzyme in the sphingolipid metabolic pathways, and it was very intriguing that silencing ASAH1 resulted in the induction of ICD. To delineate a deep understanding of the role of ASAH1, we decided to do metabolome profiling of cells after ASAH1 inhibition. An untargeted metabolomic analysis was performed for vehicle, ASAH1-KD, and LCL-521 treated CT26 and HCT116 cells using RP-positive ion mode and RP-negative ion mode. Total metabolic features (an ion with a unique retention time and m/z value) identified are 2616 from CT26 (negative mode), 3310 from HCT116 (negative mode), 4331 from HCT116 (positive mode), 3238 from CT26 (negative mode) (Fig. 4A). Online analysis software MetaboAnalyst 5.0 was used for the analysis of

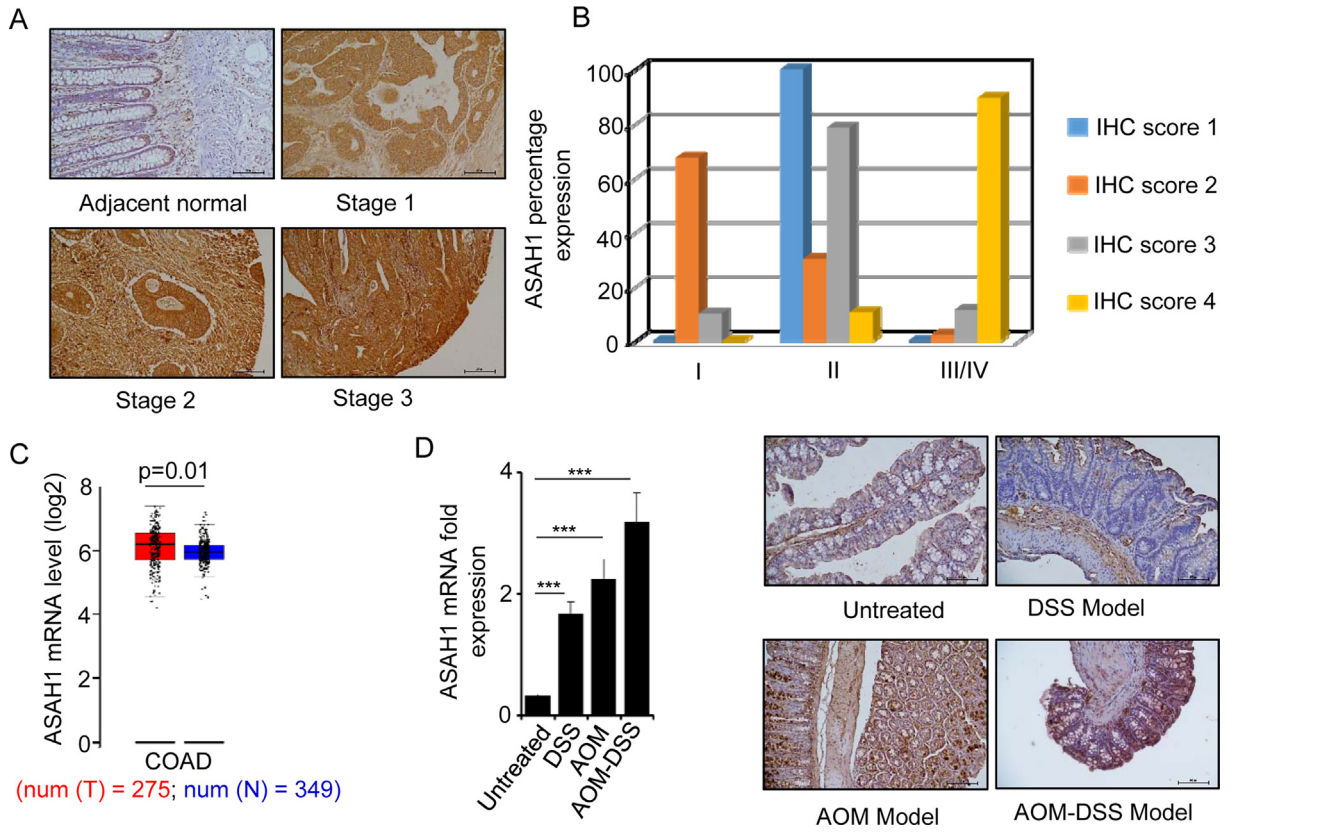

Fig. 1. ASAH1 is overexpressed in colorectal cancer. A: Representative images from immunohistochemistry analysis for ASAH1 in human colorectal cancer tissue microarray 20X magnification. **B**: IHC score and ASAH1 percentage expression in human colorectal cancer tissue microarray **C**: ASAH1 gene expression analysis in colorectal adenocarcinoma (COAD) using Gene Expression Profiling Interactive Analysis (GEPIA) based on the TCGA and GTEx database. Each box plot represents the gene expression level in terms of log2 (TPM + 1) in the tumor (red, n = 275) and normal (blue, n = 349) samples, respectively. Normal tissues were matched TCGA adjacent tissue and GTEx data. p value cutoff = 0.01. **D:** ASAH1 mRNA levels (fold change, left panel) and immunohistochemical analysis of ASAH1 (right panel) in colon samples from untreated, colitis models, azoxymethane induced colon cancer, and azoxymethane induced DSS promoted colitis-associated cancer models. Chi-squared tests examine the association between ASAH1 expression and clinical parameters. All reported p-values are two-sided and significance level was set at < 0.05 (for A). Statistical significance was calculated using ANOVA ***p < 0.001. (For interpretation of the references to color in this figure legend, the reader is referred to the web version of this article.)

the metabolomic data to find out the metabolites showing significant changes in ASAH1-KD and LCL-521 treated groups when compared to the vehicle. We observed that glutathione levels were decreased when ASAH1 expression was inhibited in both CT26 and HCT116 cell lines. To confirm this, the levels of reduced glutathione (GSH) and glutathione peroxidase (GPx) activity were assayed in the cell lines. Interestingly both GSH and GPx were reduced after LCL-521 treatment or knockdown of ASAH1 (Fig. 4B). Having seen this observation, we next analyzed the glutathione pathways components *in vivo* and observed that the GSH and GPx activity levels were significantly reduced in ASAH1 silenced groups (Fig. 4C). Inhibition of glutathione has resulted in the excessive accumulation of ROS and oxidative stress [44]. Several lines of evidence confirmed that ICD induction is associated with excessive production of ROS and ROS-dependent ER stress, which helps in efficient antigen presentation [45]. The cells were exposed to LCL-521, and ROS levels were quantified after staining the cells with H2DCFDA and analyzed using flow cytometry. LCL-521 treatment resulted in a significant increase in ROS production. Interestingly the effects were attenuated in the presence of a ROS scavenger (NAC) (Fig. 4D. Hence ASAH1 inhibition resulted in the decreased function of the glutathione system and subsequent activation of ROS production and subsequent activation of ICD.

Silencing ASAH1 induces mitochondrial stress

Mitochondria is an important hub in the activation of innate immune responses to different stimuli. We were using a Seahorse XFe96 metabolic analyzer and assayed the OCR in CT26 and HCT 116 cells with either LCL-521 treatment or ASAH1 stable knockdown. OCR measures the ability of the cells to consume oxygen to produce ATP using mito stress assay kit. In CT26 cell line, treatment with different doses of LCL-521 increased the OCR value; however, in ASAH1-KD cells, it was almost inhibited. Subsequently, we calculated basal respiration, maximal respiration, ATP production, and spare respiratory capacity. All 4 parameters were decreased, and the effects were more prominent in ASAH1-KD cells (Fig. 4E–I). Similar trends were also observed in HCT116 cells (**Supp Fig. 5**A–E). Based on these assays, we concluded that mitochondrial stress is associated with silencing the expression of ASAH1. In this study, we used the same LCL-521 doses that were found to induce ICD. As described in the previous section, the overall ATP production decreased after ASAH1 silencing; nevertheless, the ATP secretion was increased during ICD.

Targeting ASAH1 enhanced the efficacy of anti-PD1 therapy in colorectal cancer

CRC is considered a cold tumor with less infiltration of cytotoxic T cells and the presence of tumor suppressive Treg population [46]. Converting cold tumors to immunogenically hot tumors has been shown to demonstrate effective and measurable clinical outcomes and checkpoint blockade is one such strategy [47]. Since LCL-521 was demonstrated to induce immunological cell death, we decided to combine LCL-521 with an anti-PD-1 antibody to study the therapeutic benefits using CT-26 syngeneic mouse model. As seen from

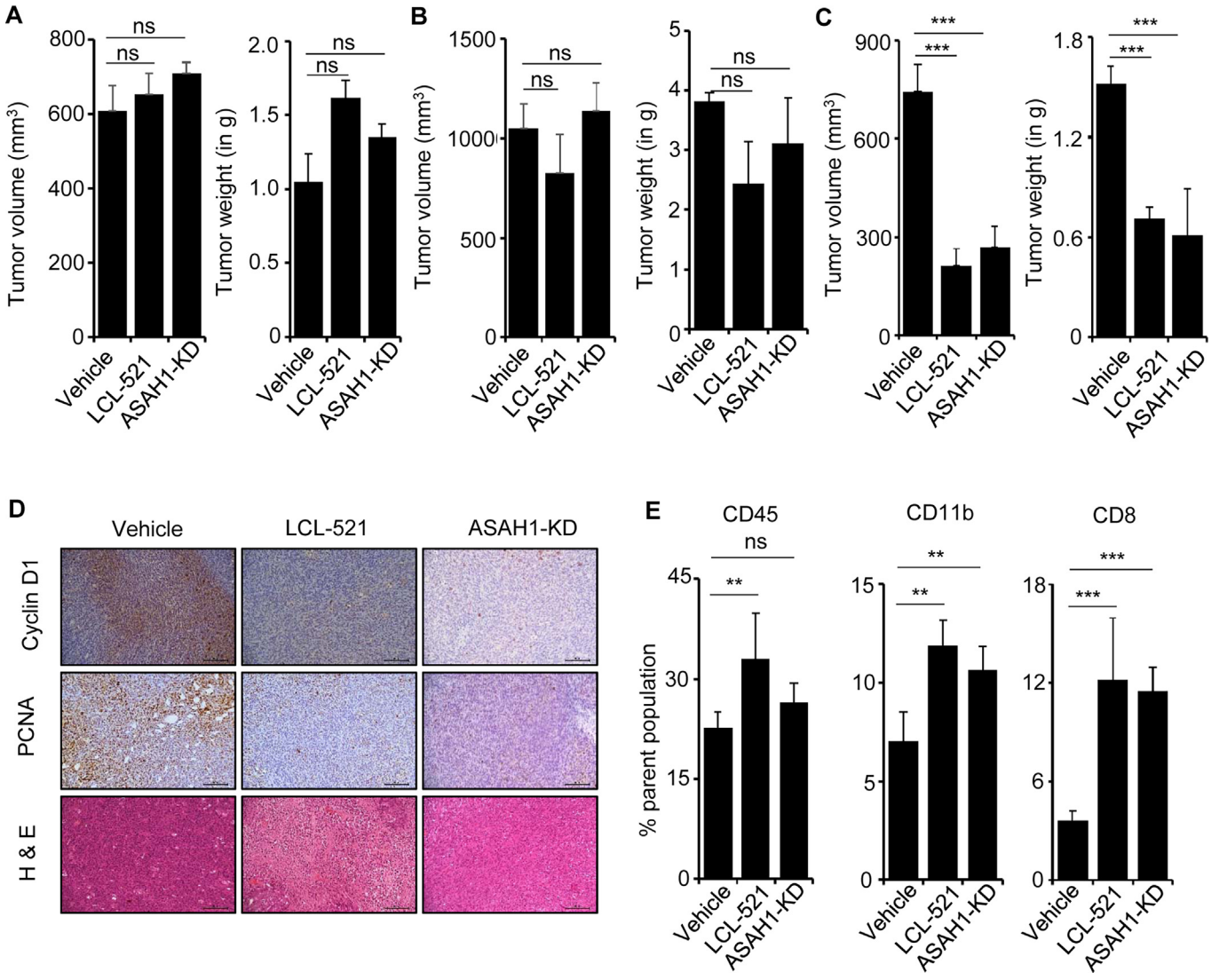

Fig. 2. Pharmacological or genetic silencing of ASAH1 inhibited colorectal cancer in syngeneic mouse models and not in immunodeficient mouse strains. A-C: NOD-SCID mice were injected with HCT116 **(A)** or CT26 **(B),** and BALB/c were injected with CT26 **(C)** (vector or ASAH1-KD cells), and one group of vector transfected cells injected group was treated with LCL-521. After sacrifice, tumor volume (left panel) and final tumor weight (right panel) were measured. Data expressed as mean ± S.D **D:** Representative images from hematoxylin-eosin stained sections and immunohistochemistry analysis for PCNA and Cyclin D1. **E:** Flow cytometric analysis of the indicated cell populations from tumor samples obtained from different treatment groups. Data expressed as mean ± S.D. Statistical significance was calculated using *t*-test $^{**}p < 0.005$, $^{***}p < 0.001$.

the final tumor volume and weight, the combination therapy resulted in further inhibition of tumor growth when compared to the individual treatments. (Fig. 5A). The expression of different proliferative markers using the immunohistochemical method (PCNA, Cyclin D1, and c-Myc) and H&E staining was done in FFPE sections (Fig. 5B). The expression of proliferative markers were decreased in LCL treated groups. The single cell suspensions were prepared from tumor samples and subjected to flow cytometric analysis after staining with various marker antibodies. CD11b was significantly upregulated in the combination group (Fig. 5C). The CD8 + T cell infiltration was elevated in the LCL-521 monotherapy and combination group, further supporting our earlier observation that silencing ASAH1 resulted in increased recruitment of CD8 T cells into the tumor microenvironment (Fig. 5D). To further understand the role of ASAH1 in infiltrating T cells, we performed intracellular cytokines staining for cytotoxic T-cell effector molecules such as interferon-gamma (IFN-γ) and granzyme B (GZB) in CD8 T cell population. Both are dramatically upregulated in LCL-521 treated groups (Fig. 5E–F). Taken together, these results suggest the impact of ASAH1 on immunotherapy outcomes.

ASAH1 silencing relieves the immunosuppression in colorectal cancer

The tumor microenvironment is mostly immunosuppressive in nature, which contributes to a greater extent of therapeutic resistance, and targeting this could make the immunologically cold tumors into immunoreactive tumors. We analyzed the expression of MDSCs ($CD11b^+F4/80^-Ly6C^+/Ly6G^+$) because they are known to be upregulated in tumors with robust immunosuppressive function [48]. We found that the monocytic subset (Ly6C +) was significantly reduced in all the treatment groups (Fig. 6A). The Treg population [49] was also evaluated, and $CD4^+FoxP3^+$ expression was significantly downregulated in the combination group (Fig. 6B). We also calculated the ratio of CD8 + T cells to FoxP3 and found that ratio was significantly increased in LCL-521 treated groups (**Supp Fig. 6**A). Multiple studies using different cancer subtypes, including CRC, showed that a higher CD8 to FoxP3 ratio favors better overall survival and is an independent predictor of clinical benefit with PD-1 inhibition [50]. Tumor-associated macrophages (TAMs) can be either pro- or anti-inflammatory in nature. When we analyzed $CD11b^+F4/80^+$ macrophages, we observed a

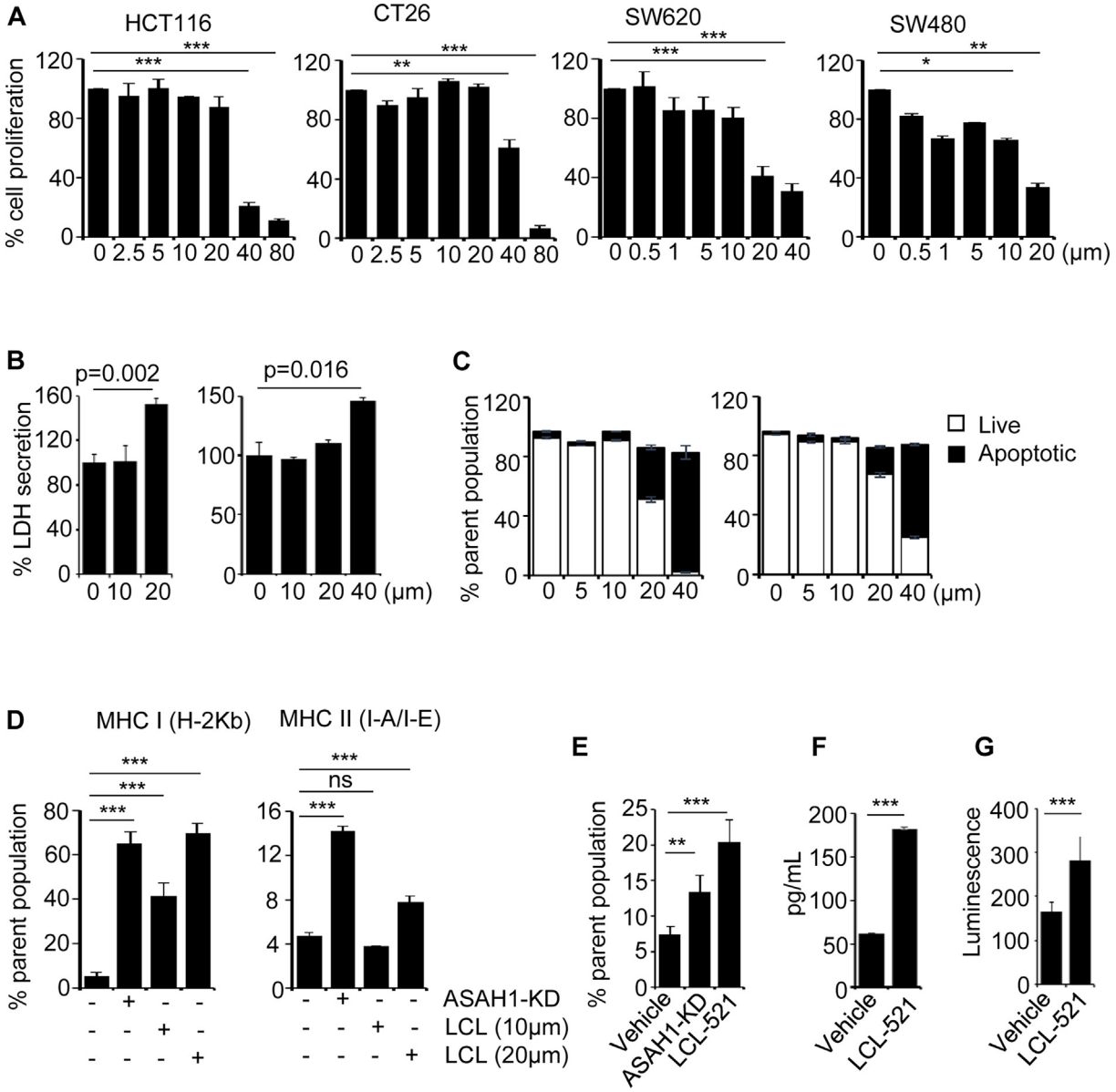

Fig. 3. Silencing of ASAH1 induces immunological cell death and MHC activation in colorectal cancer cell lines. A: Different mouse and human CRC cell lines were treated with LCL-521, and cytotoxicity was analyzed for 24 hrs. **B:** The secretion of LDH was measured in cell supernatants after 24 h in CT 26 (left panel) and HCT116 (right panel) cell lines after treatment with LCL-521. **C:** The cells, after treatment with LCL-521, were stained with Annexin V FITC and PI, and live and apoptotic populations were analyzed using FACS. **D:** Flowcytometric analysis of MHCI and MHCII positive cell population in CT26 wild type cells treated with indicated doses of LCL-521 for 24 hr, and CT26-ASAH1-KD cells **E:** The surface level expression of calreticulin was analyzed by flow cytometry in CT26 cell lines and expressed as % of the parent population. **F:** The secretion of HMBG1 (pg/ml) was assayed in CT26 cell lines by ELISA. **G:** The release of ATP was assayed using a luminescence based method. Data expressed as mean ± S.D. Statistical significance was calculated using ANOVA *p < 0.05, **p < 0.005, ***p < 0.001.

striking upregulation in all the treatment groups (Fig. 6C). The macrophages are important for the clearance of cell debris, and we observed significant cell death in treatment groups; hence we presumed that the observed increase in F4/80 + cells is favoring the host immune system in eradicating the tumor. To confirm, we checked the expression M1 macrophage markers (CD11b, CD80, CD86, and iNOS), and there was an upregulation of these markers after LCL-521 treatment. This further confirms that silencing ASAH1 increased the M1 macrophage population (**Supp Fig. 6**B–D). To elucidate the potential association between ASAH1 and immune cell infiltration, we selected 300 samples from the TCGA data set for COAD and selected 10 % of patients who showed high and low expression of ASAH1. The levels of M1, and M2 macrophages and Treg were analyzed using TIMER 2.0 database. The results demonstrated that expression of ASAH1 positively correlates with Treg and M2 Macrophages infiltration but not with M1 macrophages (**Supp Fig. 6**E–G). This indicates that ASAH1 can modulate intra-tumoral M1/M2 balance, and inhibiting ASAH1 shifts the equilibrium towards a more pro-inflammatory M1 phenotype, thereby increasing the antitumor response. Several studies have shown that increased levels of M2 macrophages are associated with decreased survival of patients in different cancer types [51,52]. Next, we performed a quantitative gene expression of a subset of genes known to be involved in antigen presentation and MHC function (B2N, PSMB8, CD74, LGMN). The selected panel of genes was significantly upregulated in LCL-521 treated groups (Fig. 6D). These results unequivocally confirmed that targeting ASAH1 reprograms the highly immunosuppressive tumor microenvironment into an immunoreactive phenotype leading to the inhibition of the tumor.

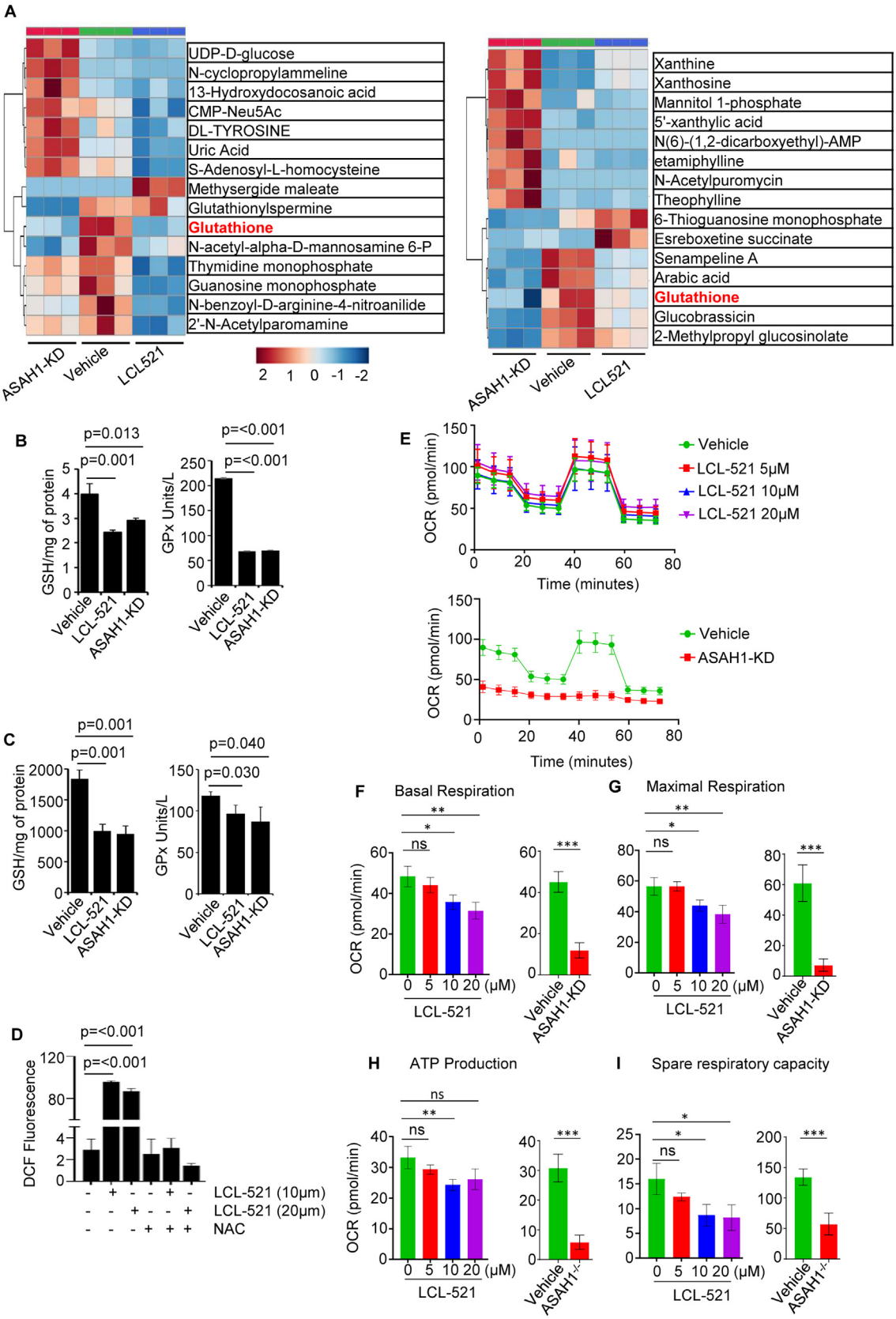

Fig. 4. ASAH1 inhibition resulted in mitochondrial stress, a decrease in the glutathione system, and ROS production. A: Metabolomic analysis of CT26 (left panel) and HCT116 (right panel). Heat map of differential metabolites (upregulated and downregulated) identified through metabolomics analysis and metabolic pathway analysis. In the heat map, the row displays metabolite, and the column represents the samples (in triplicate). **B-C:** Analysis of total GSH and GPx levels in CT26 cell lines **(B)** and in tumor samples **(C)** from the BALB/c model. **D:** The ROS production was assayed using flow cytometry in the presence of LCL-521 or in combination with NAC after 24hr of treatment. **E-I:** Oxygen Consumption Rate (OCR) measurements were calculated over a period of time (min) using a Seahorse analyzer in the CT26 cell line. **E:** oxygen consumption rate (OCR), **F:** basal respiration; **G:** maximal respiration; **H:** ATP production; **I:** spare respiratory capacity, calculated as the difference between maximal and basal OCR. Data expressed as mean ± S.D. Statistical significance was calculated using ANOVA *p < 0.05, **p < 0.005, ***p < 0.001.

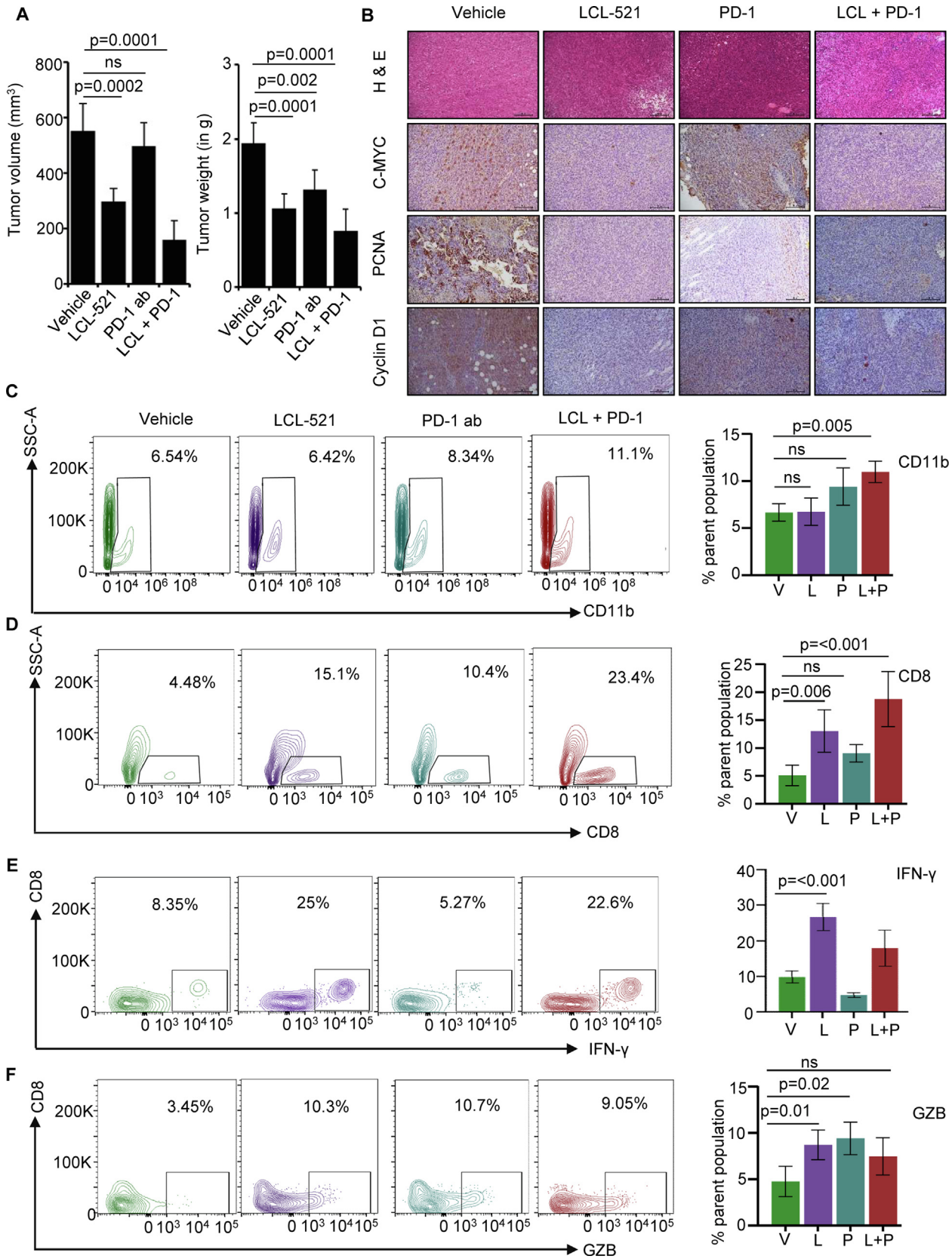

Fig. 5. LCL-521 sensitizes colorectal cancer to PD-1 antibody therapy in syngeneic mouse tumor model. A: BALB/c mice were injected with CT26 and treated with either LCL-521 or PD-1 antibody or in combination. The final tumor volume in mm^3 (left panel) and tumor weight in grams (right panel). **B:** Representative images of H&E-stained sections. Proliferative markers such as c-Myc, PCNA, and Cyclin D1 expression were evaluated using immunohistochemistry. **C-F:** Single cell suspensions from tumors obtained from the experimental groups were stained with the indicated antibodies and analyzed by flowcytometry. The left panels show a representative contour plot per experimental group. The bar graph on the right panel is the average of 3–4 mice in each group. CD11b levels are shown in **C**. and CD8 + T cell infiltration in **D**. The intracellular cytokine staining of cytotoxic T-cell effector molecules IFN-γ **(E)** and granzyme B (GZB) **(F)** levels in tumor samples from the experimental groups were analyzed using flowcytometry and expressed in percentage population of CD8 + T cells. Data expressed as mean ± S.D. Statistical significance was calculated using ANOVA $^{*}p < 0.05$, $^{**}p < 0.005$, $^{***}p < 0.001$.

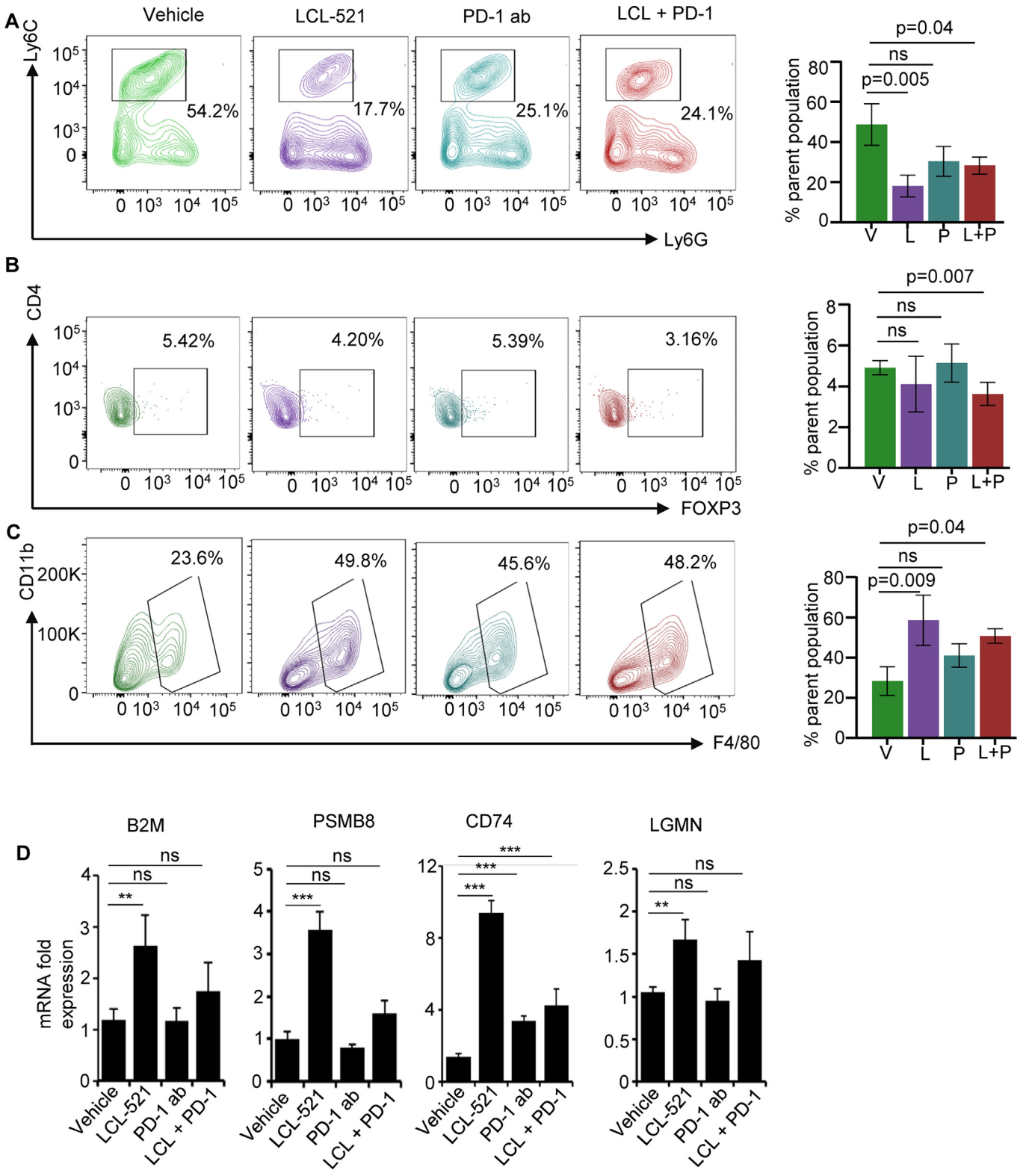

Fig. 6. LCL-521 inhibited the expression of MDSCs and Tregs and activates macrophage recruitment and the expression of genes involved in antigen presentation. A-B: MDSCs **(A)** and Tregs **(B)** expression were analyzed in tumor samples using flow cytometry. **C**: The macrophage recruitment was assessed based on the staining with CD11b + F4/80 + markers. **D:** The expression of genes was analyzed in the tumor samples from the experimental groups by q-RT PCR. GAPDH served as the housekeeping gene. Data expressed as mean ± S.D (A, B, C) and mean ± SEM (D). Statistical significance was calculated using ANOVA *p < 0.05, **p < 0.005, ***p < 0.001.

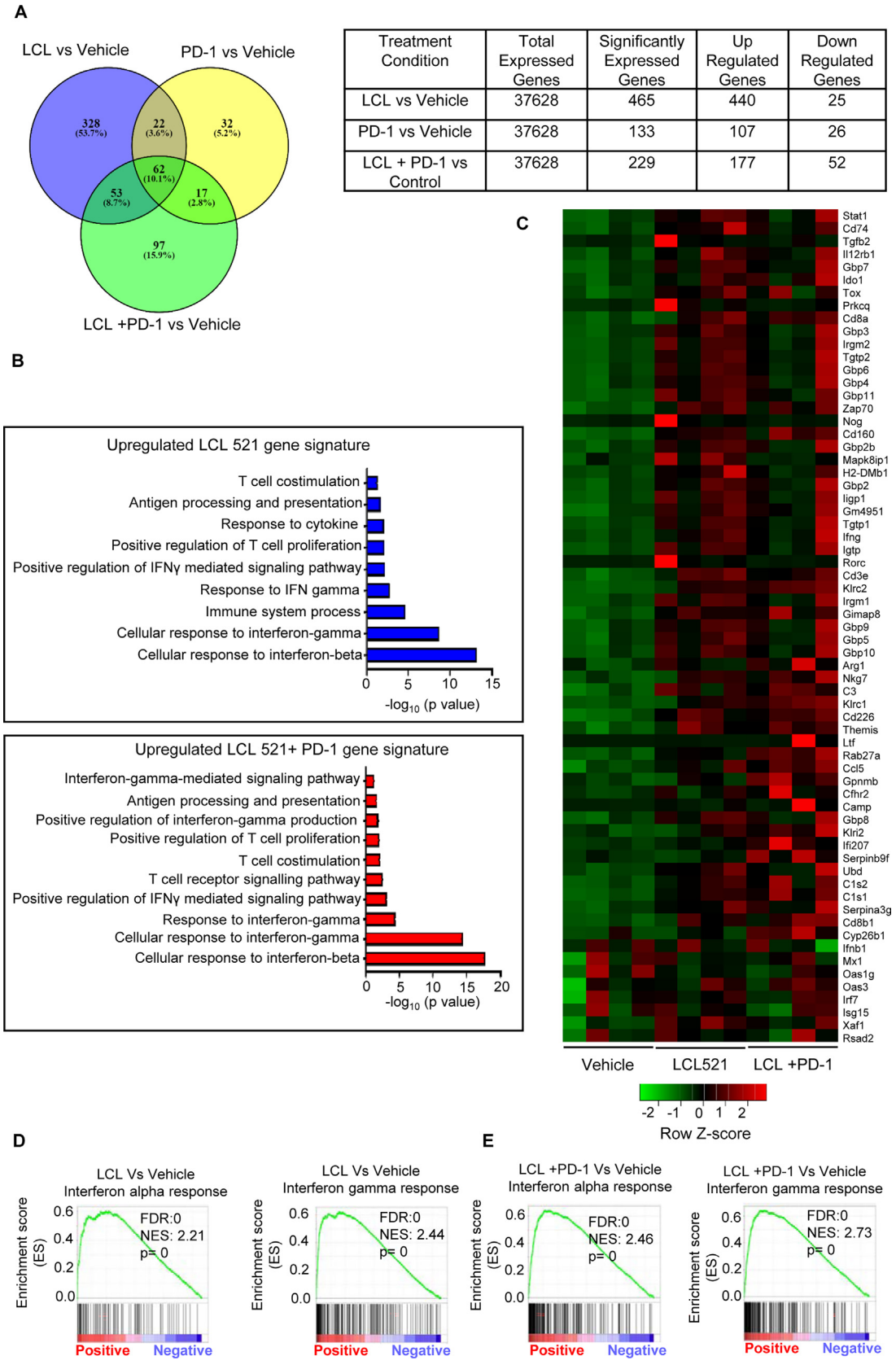

Treatment Condition	Total Expressed Genes	Significantly Expressed Genes	Up Regulated Genes	Down Regulated Genes
LCL vs Vehicle	37628	465	440	25
PD-1 vs Vehicle	37628	133	107	26
LCL + PD-1 vs Control	37628	229	177	52

Fig. 7. LCL-521 treatment induces type I and II interferon response in the tumor microenvironment. A: Venn diagram and a table summarizing the differentially expressed genes and overlap of significantly differentially expressed genes in different treatment groups. **B:** The top upregulated functional pathways determined by Gene Ontology analysis in the LCL-521 monotherapy and LCL-521 + PD1 combination groups. **C:** Heatmap showing expression of type I and II interferon (IFN) response genes, which were significantly upregulated. **D:** GSEA of IFN α and γ in LCL-521 monotherapy group. **E:** GSEA of IFN α and γ in LCL-521 + PD-1 combination group (NES, normalized enrichment score; FDR, false discovery rate).

LCL-521 treatment resulted in a strong type I and II IFN response within the tumor milieu

At this juncture, we performed an RNA sequencing analysis to elucidate a detailed understanding of various pathways that get altered during LCL-521 treatment. The differential gene expression patterns are given in Fig. 7A. We noticed a striking upregulation of type I and II interferon response after LCL-521 treatment. When the pathway analysis was done, the top functional gene categories were related to the cellular response to interferon-beta and Cellular response to interferon-gamma in LCL-521 alone treated group and in combination group (Fig. 7B). The heatmap of a subset of genes differentially expressed were shown in Fig. 7C. The major class of genes (Ifnb1, Mx1, Oas1g, Oas3, Irf7, CCl5, IsG15, Xaf1, Rsad2 etc.) were involved in the cellular processes such as modulation of antiviral immunity, production of cytokines and chemokines, T cell costimulatory molecules and immune cell activation and function. To further characterize the biological processes underlying the transcriptional changes, gene set enrichment analysis (GSEA) analysis was performed using the MSigDB hallmark gene set collection [53]. From the analysis, we noticed a profound enrichment of "IFN α and γ response" and many other immune related and inflammatory pathways (Fig. 7D–E). GSEA analysis was performed on RNA sequencing samples to assess the altered gene sets in all the treatment groups compared to the control group. We found that the treatment with LCL-521 alone significantly enriched IFN-α and IFN-γ signaling. This is further increased in combination with the PD-1 antibody. The significantly upregulated pathways, according to GSEA analysis, are shown in **Suppl Table 3–4**. This shows that the blockade of ASAH1 signaling alone can impact the tumor microenvironment by increasing CD8 + T cell infiltration and higher IFN signaling.

Discussion

Acid ceramidase, which converts ceramide to sphingosine, was found to be overexpressed in different types of cancer. In this study, we demonstrated that ASAH1 provided survival advantages to tumor cells by modulating the tumor microenvironment. In vitro studies confirmed that inhibition of ASAH1 resulted in immunological cell death and activation of MHC molecules. The syngeneic tumor models confirmed that LCL-521 treatment enhanced the infiltration of CD8 + T cells and M1 macrophages. A study by Junior et al showed that treatment of macrophages with ceramide increased expression of the CD68 (a marker of M1phenotype) and inhibited the expression of the CD163 (M2 marker) and IL-10 secretion indicating that ceramide can prevent M2 polarization [54]. A decrease in ceramide levels promotes Treg differentiation and interferes with the cytotoxic activity of CD8 + T cells [55]. In a mice model where ASAH1 is silenced in T cells, increased accumulation of ceramide enhanced the cytotoxic potential of CD8 T cells [55]. These two studies support our observation of the effect of ASAH1 in CD8T cells.

Together with the induction of ICD, we also noticed that silencing of ASAH1 resulted in mitochondrial stress, increased the production of ROS and ATP secretion, and impairment of the glutathione system. Several studies have independently confirmed that mito stress led to the activation of the innate immune response, mtDNA can act as DAMP leading to the induction of interferon response in human and mice models [56]. In pancreatic cancer cells, also knockdown of ASAH1 resulted in mitochondrial dysfunction, ROS production, and apoptosis [21]. More studies are required to elucidate a detailed mechanism of ASAH1 dependent regulation of mitochondrial function.

In tumors with low immune response, a combination of ICD inducers and checkpoint inhibitor-based therapy is gaining wide attention. In lung cancer, co-administration of the ICD-inducing chemotherapeutics (oxaliplatin and cyclophosphamide) sensitized the tumors to anti-PD1 and anti-CTLA4 therapy [57]. Dinaciclib, a CDK inhibitor and ICD inducer, sensitized the mouse tumors to anti-PD1, which resulted in increased T cell infiltration and DC activation [58]. Currently, several clinical trials are ongoing with a combination of checkpoint inhibitors and ICD inducers [13]. Targeting sphingolipid metabolizing enzymes is gaining considerable interest in the development of new therapeutics against cancer due it its multifaceted role in cellular metabolism [59]. Sphingolipid analysis of therapy resistant tumors reported decreased levels of ceramides. Considering the established role of ceramides in cell death in resistant tumors elevating the levels of ceramides will make them susceptible to therapy [60]. Targeting ASAH1 will be one such approach because this enzyme converts Ceramide to Sphingosine.

Conclusion

In conclusion, for the first time, our study demonstrates that ASAH1 is overexpressed in colorectal cancer, and silencing the expression resulted in the induction of ICD, decrease in glutathione system, Increase in mitochondrial stress, and ROS production. The ASAH1 inhibitor (LCL-521), either as monotherapy or in combination with an anti-PD-1 antibody, resulted in (a) better regression of tumors; (b) an activation of M1 macrophages and T cells; (c) which led to enhanced infiltration of cytotoxic T cells and (d) suppression of MDSCs and Tregs and (e) induction of type I and II IFN response. Our findings provide strong pre-clinical efficacy data for the combination of LCL-521 and ICIs, which led to the sensitization of immunologically cold tumors into immune reactive hot tumors.

Declarations

Ethics approval and consent to participate.
Not applicable.

Consent for publication

Not applicable.

Availability of data and materials

The datasets generated during the current study are available from the corresponding author upon reasonable request. The transcriptomic data set is deposited in NCBI-SRA.

Funding

The work is supported by SERB core research grant (CRG/2022/004283) and in part by RGCB-laboratory research fund and DBT-Ramalingaswami fellowship (No. BT/RLF/Reentry/38/2011) to KBH.

CRediT authorship contribution statement

Yadu Vijayan: Conceptualization, Methodology, Formal analysis, Investigation, Writing – review & editing. **Shirley James:** Methodology, Formal analysis, Investigation, Validation. **Arun Viswanathan:** Methodology, Formal analysis, Investigation. **Jayasekharan S Aparna:** Methodology, Formal analysis, Investigation. **Anu Bindu:** Formal analysis, Investigation. **Narayanan N**

Namitha: Investigation. **Devasena Anantharaman:** Formal analysis, Investigation, Data curation, Visualization. **Manendra Babu Lankadasari:** Conceptualization, Formal analysis, Investigation, Data curation, Visualization. **Kuzhuvelil B Harikumar:** Conceptualization, Methodology, Formal analysis, Resources, Investigation, Visualization, Supervision, Project administration, Funding acquisition, Writing – review & editing.

Declaration of competing interest

The authors declare that they have no known competing financial interests or personal relationships that could have appeared to influence the work reported in this paper.

Acknowledgments

YV and AV acknowledge research fellowships from CSIR and University Grant Commission, respectively. We express our sincere gratitude to the personnel of RGCB core facilities (Animal research facility, Central histology core, FACS core facility, Bio-imaging facility and DBT-SAHAJ National Facility for Mass Spectrometry-Based Proteomics, Metabolomics and Lipidomics Platforms) for their excellent technical assistance. Clevergene, Bangalore for transcriptomic analysis. YV acknowledge the doctoral advisory committee for their valuable suggestions.

Appendix A. Supplementary data

Supplementary data to this article can be found online at https://doi.org/10.1016/j.jare.2023.12.013.

References

[1] Anderson NM, Simon MC. The tumor microenvironment. Curr Biol 2020;30:R921–5.
[2] Hinshaw DC, Shevde LA. The tumor microenvironment innately modulates cancer progression. Cancer Res 2019;79:4557–66.
[3] Aldea M, Andre F, Marabelle A, Dogan S, Barlesi F, Soria JC. Overcoming resistance to tumor-targeted and immune-targeted therapies. Cancer Discov 2021;11:874–99.
[4] Coulie PG, Van den Eynde BJ, van der Bruggen P, Boon T. Tumour antigens recognized by T lymphocytes: At the core of cancer immunotherapy. Nat Rev Cancer 2014;14:135–46.
[5] Brochier W, Bricard O, Coulie PG. Facts and hopes in cancer antigens recognized by T cells. Clin Cancer Res 2023;29:309–15.
[6] Bagchi S, Yuan R, Engleman EG. Immune checkpoint inhibitors for the treatment of cancer: Clinical impact and mechanisms of response and resistance. Annu Rev Pathol 2021;16:223–49.
[7] Christenson ES, Meyer J. Is PD-1 inhibitor monotherapy a new standard treatment for MMR-deficient locally advanced rectal cancer? Curr Oncol Rep 2022;24:1373–5.
[8] Lu J, Tai Z, Wu J, Li L, Zhang T, Liu J, et al. Nanomedicine-induced programmed cell death enhances tumor immunotherapy. J Adv Res 2023.
[9] Boukouris AE, Theochari M, Stefanou D, Papalambros A, Felekouras E, Gogas H, et al. Latest evidence on immune checkpoint inhibitors in metastatic colorectal cancer: A 2022 update. Crit Rev Oncol Hematol 2022;173:103663.
[10] Jia Y, Liu L, Shan B. Future of immune checkpoint inhibitors: Focus on tumor immune microenvironment. Ann Transl Med 2020;8:1095.
[11] Zhang C, Zhang C, Wang H. Immune-checkpoint inhibitor resistance in cancer treatment: Current progress and future directions. Cancer Lett 2023;562:216182.
[12] Sprooten J, Laureano RS, Vanmeerbeek I, Govaerts J, Naulaerts S, Borras DM, et al. Trial watch: chemotherapy-induced immunogenic cell death in oncology. Oncoimmunology 2023;12.
[13] Shi F, Huang X, Hong Z, Lu N, Huang X, Liu L, et al. Improvement strategy for immune checkpoint blockade: A focus on the combination with immunogenic cell death inducers. Cancer Lett 2023;562:216167.
[14] Coant N, Sakamoto W, Mao C, Hannun YA. Ceramidases, roles in sphingolipid metabolism and in health and disease. Adv Biol Regul 2017;63:122–31.
[15] Vijayan Y, Lankadasari MB, Harikumar KB. Acid ceramidase: A novel therapeutic target in cancer. Curr Top Med Chem 2019;19:1512–20.
[16] Sugita M, Dulaney JT, Moser HW. Ceramidase deficiency in Farber's disease [lipogranulomatosis]. Science 1972;178:1100–2.
[17] Zhou J, Tawk M, Tiziano FD, Veillet J, Bayes M, Nolent F, et al. Spinal muscular atrophy associated with progressive myoclonic epilepsy is caused by mutations in ASAH1. Am J Hum Genet 2012;91:5–14.
[18] Newton J, Lima S, Maceyka M, Spiegel S. Revisiting the sphingolipid rheostat: Evolving concepts in cancer therapy. Exp Cell Res 2015;333:195–200.
[19] Roh JL, Park JY, Kim EH, Jang HJ. Targeting acid ceramidase sensitises head and neck cancer to cisplatin. Eur J Cancer 2016;52:163–72.
[20] Liu X, Cheng JC, Turner LS, Elojeimy S, Beckham TH, Bielawska A, et al. Acid ceramidase upregulation in prostate cancer: Role in tumor development and implications for therapy. Expert Opin Ther Targets 2009;13:1449–58.
[21] Taniai T, Shirai Y, Shimada Y, Hamura R, Yanagaki M, Takada N, et al. Inhibition of acid ceramidase elicits mitochondrial dysfunction and oxidative stress in pancreatic cancer cells. Cancer Sci 2021;112:4570–9.
[22] Tan SF, Pearson JM, Feith DJ, Loughran Jr TP. The emergence of acid ceramidase as a therapeutic target for acute myeloid leukemia. Expert Opin Ther Targets 2017;21:583–90.
[23] Doan NB, Nguyen HS, Al-Gizawiy MM, Mueller WM, Sabbadini RA, Rand SD, et al. Acid ceramidase confers radioresistance to glioblastoma cells. Oncol Rep 2017;38:1932–40.
[24] Beckham TH, Cheng JC, Lu P, Marrison ST, Norris JS, Liu X. Acid ceramidase promotes nuclear export of PTEN through sphingosine 1-phosphate mediated Akt signaling. PLoS One 2013;8:e76593.
[25] Bowden DL, Sutton PA, Wall MA, Jithesh PV, Jenkins RE, Palmer DH, et al. Proteomic profiling of rectal cancer reveals acid ceramidase is implicated in radiation response. J Proteomics 2018;179:53–60.
[26] Clifford RE, Govindarajah N, Bowden D, Sutton P, Glenn M, Darvish-Damavandi M, et al. Targeting acid ceramidase to improve the radiosensitivity of rectal cancer. Cells 2020;9.
[27] Lankadasari MB, Aparna JS, Mohammed S, James S, Aoki K, Binu VS, et al. Targeting S1PR1/STAT3 loop abrogates desmoplasia and chemosensitizes pancreatic cancer to gemcitabine. Theranostics 2018;8:3824–40.
[28] James S, Aparna JS, Paul AM, Lankadasari MB, Mohammed S, Binu VS, et al. Cardamonin inhibits colonic neoplasia through modulation of MicroRNA expression. Sci Rep 2017;7:13945.
[29] Mohammed S, Vineetha NS, James S, Aparna JS, Babu Lankadasari M, Maeda T, et al. Regulatory role of SphK1 in TLR7/9-dependent type I interferon response and autoimmunity. FASEB J 2020;34:4329–47.
[30] Moron MS, Depierre JW, Mannervik B. Levels of glutathione, glutathione reductase and glutathione S-transferase activities in rat lung and liver. Biochim Biophys Acta 1979;582:67–78.
[31] Hafeman DG, Sunde RA, Hoekstra WG. Effect of dietary selenium on erythrocyte and liver glutathione peroxidase in the rat. J Nutr 1974;104:580–7.
[32] Kumar AA, Satheesh G, Vijayakumar G, Chandran M, Prabhu PR, Simon L, et al. Postprandial metabolism is impaired in overweight normoglycemic young adults without family history of diabetes. Sci Rep 2020;10:353.
[33] Divakaruni AS, Jastroch M. A practical guide for the analysis, standardization and interpretation of oxygen consumption measurements. Nat Metab 2022;4:978–94.
[34] James S, Aparna JS, Babu A, Paul AM, Lankadasari MB, Athira SR, et al. Cardamonin attenuates experimental colitis and associated colorectal cancer. Biomolecules 2021;11.
[35] Bai A, Mao C, Jenkins RW, Szulc ZM, Bielawska A, Hannun YA. Anticancer actions of lysosomally targeted inhibitor, LCL521, of acid ceramidase. PLoS One 2017;12.
[36] Schmid MC, Khan SQ, Kaneda MM, Pathria P, Shepard R, Louis TL, et al. Integrin CD11b activation drives anti-tumor innate immunity. Nat Commun 2018;9:5379.
[37] Eriksen AC, Sorensen FB, Lindebjerg J, Hager H, dePont Christensen R, Kjaer-Frifeldt S, et al. The prognostic value of tumor-infiltrating lymphocytes in stage II colon cancer. A nationwide population-based study. Transl Oncol 2018;11:979–87.
[38] Kumar P, Nagarajan A, Uchil PD. Analysis of cell viability by the lactate dehydrogenase assay. Cold Spring Harb Protoc 2018;2018.
[39] Krysko DV, Garg AD, Kaczmarek A, Krysko O, Agostinis P, Vandenabeele P. Immunogenic cell death and DAMPs in cancer therapy. Nat Rev Cancer 2012;12:860–75.
[40] Galluzzi L, Vitale I, Warren S, Adjemian S, Agostinis P, Martinez AB, et al. Consensus guidelines for the definition, detection and interpretation of immunogenic cell death. J Immunother Cancer 2020;8.
[41] Fucikova J, Spisek R, Kroemer G, Galluzzi L. Calreticulin and cancer. Cell Res 2021;31:5–16.
[42] Chen R, Kang R, Tang D. The mechanism of HMGB1 secretion and release. Exp Mol Med 2022;54:91–102.
[43] Fucikova J, Kepp O, Kasikova L, Petroni G, Yamazaki T, Liu P, et al. Detection of immunogenic cell death and its relevance for cancer therapy. Cell Death Dis 2020;11:1013.
[44] Forman HJ, Zhang H, Rinna A. Glutathione: overview of its protective roles, measurement, and biosynthesis. Mol Aspects Med 2009;30:1–12.
[45] Zhou J, Wang G, Chen Y, Wang H, Hua Y, Cai Z. Immunogenic cell death in cancer therapy: Present and emerging inducers. J Cell Mol Med 2019;23:4854–65.
[46] Liu JL, Yang M, Bai JG, Liu Z, Wang XS. "Cold" colorectal cancer faces a bottleneck in immunotherapy. World J Gastrointest Oncol 2023;15:240–50.

[47] Weng J, Li S, Zhu Z, Liu Q, Zhang R, Yang Y, et al. Exploring immunotherapy in colorectal cancer. J Hematol Oncol 2022;15:95.
[48] Wu Y, Yi M, Niu M, Mei Q, Wu K. Myeloid-derived suppressor cells: an emerging target for anticancer immunotherapy. Mol Cancer 2022;21:184.
[49] Iglesias-Escudero M, Arias-Gonzalez N, Martinez-Caceres E. Regulatory cells and the effect of cancer immunotherapy. Mol Cancer 2023;22:26.
[50] Tavares MC, Sampaio CD, Lima GE, Andrade VP, Goncalves DG, Macedo MP, et al. A high CD8 to FOXP3 ratio in the tumor stroma and expression of PTEN in tumor cells are associated with improved survival in non-metastatic triple-negative breast carcinoma. BMC Cancer 2021;21:901.
[51] Lan C, Huang X, Lin S, Huang H, Cai Q, Wan T, et al. Expression of M2-polarized macrophages is associated with poor prognosis for advanced epithelial ovarian cancer. Technol Cancer Res Treat 2013;12:259–67.
[52] Yang C, Wei C, Wang S, Shi D, Zhang C, Lin X, et al. Elevated CD163(+)/CD68(+) ratio at tumor invasive front is closely associated with aggressive phenotype and poor prognosis in colorectal cancer. Int J Biol Sci 2019;15:984–98.
[53] Liberzon A, Birger C, Thorvaldsdottir H, Ghandi M, Mesirov JP, Tamayo P. The molecular signatures database (MSigDB) hallmark gene set collection. Cell Syst 2015;1:417–25.
[54] de Araujo Junior RF, Eich C, Jorquera C, Schomann T, Baldazzi F, Chan AB, et al. Ceramide and palmitic acid inhibit macrophage-mediated epithelial-mesenchymal transition in colorectal cancer. Mol Cell Biochem 2020;468:153–68.
[55] Hose M, Gunther A, Naser E, Schumacher F, Schonberger T, Falkenstein J, et al. Cell-intrinsic ceramides determine T cell function during melanoma progression. Elife 2022;11.
[56] Song Y, Zhou Y, Zhou X. The role of mitophagy in innate immune responses triggered by mitochondrial stress. Cell Commun Signal 2020;18:186.
[57] Pfirschke C, Engblom C, Rickelt S, Cortez-Retamozo V, Garris C, Pucci F, et al. Immunogenic chemotherapy sensitizes tumors to checkpoint blockade therapy. Immunity 2016;44:343–54.
[58] Hossain DMS, Javaid S, Cai M, Zhang C, Sawant A, Hinton M, et al. Dinaciclib induces immunogenic cell death and enhances anti-PD1-mediated tumor suppression. J Clin Invest 2018;128:644–54.
[59] Ung J, Tan SF, Fox TE, Shaw JJP, Vass LR, Costa-Pinheiro P, et al. Harnessing the power of sphingolipids: Prospects for acute myeloid leukemia. Blood Rev 2022;55:100950.
[60] Gomez-Munoz A. The role of ceramide 1-Phosphate in tumor cell survival and dissemination. Adv Cancer Res 2018;140:217–34.